ELSEVIER

Journal of Nuclear Materials 254 (1998) 143–150

journal of nuclear materials

# Small angle neutron scattering investigations of the microstructure of VVER-440-type reactor pressure vessel steel after irradiation at 60°C

M. Grosse [a,*], J. Boehmert [a], R. Gilles [b]

[a] *Forschungszentrum Rossendorf, P.O. Box 510 119, D-01314 Dresden, Germany*
[b] *Hahn-Meitner-Institut Berlin, Glienicker Str. 100, D-14109 Berlin, Germany*

Received 12 September 1997; accepted 14 January 1998

**Abstract**

The formation of point defects and precipitates after neutron irradiation of VVER-440-type reactor pressure vessel steel was investigated by small angle neutron scattering experiments. Irradiation at 60°C increased the number of point defects, decreased the precipitates, which already exist in the unirradiated state, and formed a new type of fine-scaled precipitates. Post-irradiation annealing near the operational temperature of the nuclear power plants (270°C) provoked a slight decrease of the content of point defects and of the irradiation-induced precipitates. The content of these precipitates which are also present in the unirradiated state did not change by annealing. © 1998 Elsevier Science B.V.

## 1. Introduction

The microstructural damage process causing neutron embrittlement of reactor pressure vessel (RPV) steels proceeds in two general stages:

1. formation of displacement cascades,
2. evolution of the defect microstructure.

In the first stage, atoms are removed by multiple collision from their places in the iron lattice as well as in the precipitates. Finally, a large number of Frenkel pairs, or isolated point defects (vacancies, interstitial self or solute atoms), and vacancy rich displacement cascade cores are created [1]. As a consequence, partial or complete dissolution of precipitates can occur [2]. The processes mainly depend on the material (crystal structure, chemical composition) and on the irradiation parameters (neutron spectrum, dose, dose rate). But they only weakly depend on the temperature.

In the second stage, the surviving point defects and super-small clusters can be rearranged by diffusion processes. They can be annihilated by recombination, can be trapped in sinks like grain boundaries, voids, interfaces or dislocations, and can form dislocation loops. Preferably, the system will enter into a permanent non-equilibrium state with a high point defect supersaturation. This yields irradiation-enhanced or irradiation-induced precipitation. All these processes are strongly influenced by the irradiation temperature.

Thus, the investigation of the microstructural evolution produced by irradiation at different temperatures can be useful to understand the irradiation damaging of RPV steels. Recently some results have been presented for low temperature irradiation.

This paper concerns small angle neutron scattering (SANS) analysis of the microstructure of VVER-440-type RPV steel after neutron irradiation at 60°C. It is a bainitic Cr–Mo–V steel with the Russian designation 15 Kh2MFA.

## 2. Materials and measurements

The study used two laboratory heats ESW-A and -C (see Table 1). They differ primarily in their content of copper but also of silicon, vanadium, chromium and manganese. Their chemical compositions correspond to the VVER-440-type RPV steel 15 Kh2MFA. The thermal treatment of these materials is similar to the industrial

* Corresponding author. Tel.: +49-351 260 3155; fax: +49-351 260 2205.


*PII* S0022-3115(98)00013-0

Table 1
Chemical composition (in at.%) of the used materials (Fe: balance)

| Material code | C | N | Si | P | V | Cr | Mn | Ni | Cu | Mo |
|---|---|---|---|---|---|---|---|---|---|---|
| ESW-A | 0.67 | 0.07 | 0.27 | 0.03 | 0.24 | 2.45 | 0.27 | 0.07 | 0.12 | 0.39 |
| ESW-C | 0.67 | 0.07 | 0.35 | 0.03 | 0.33 | 2.78 | 0.36 | 0.06 | .29 | 0.39 |

Table 2
Irradiation conditions in the reactor RFR Rossendorf

| Material | Fluence ($cm^{-2}$) ($E > 1$ MeV) | dpa | Temp. (°C) |
|---|---|---|---|
| ESW-A | $23\times10^{18}$ | 0.031 | 60 |
| ESW-C | $11\times10^{18}$ | 0.015 | 60 |

manufacturing procedure of this steel. It comprises austenitization at 1000°C for 1 h in argon atmosphere, quenching in oil, tempering at 700°C for 10 h in argon, and final cooling in air. The samples were irradiated at the Research Reactor Rossendorf (RFR). The irradiation conditions of the test materials are given in Table 2.

Samples with a thickness of about 1 mm were cut from half Charpy-V specimens of these materials in the unirradiated and the irradiated state. Some of the irradiated samples were annealed for 1 h at 270°C in argon.

The SANS investigations were performed at the SANS-V4 facility at the BER-II research reactor of the Berlin Neutron Scattering Center BENSC [3] with a neutron wavelength of 0.6 nm. The scattering vector ranged between 0.2 $nm^{-1} \le \boldsymbol{Q} \le 3.0\ nm^{-1}$. During the experiments the samples were magnetized in a magnetic field of 1.4 T. This magnetic field is strong enough to reach the saturation magnetization in the samples [4]. For the background correction, the empty holders were measured. The absolute calibration was performed by measurements of a water standard. A two-dimensional position sensitive detector, consisting of $64 \times 64$ cells with a size of 1 cm $\times$ 1 cm, was used to measure the scattering intensity. BENSC provided the software packet required for calibration, correction of detector sensitivity and background and radial averaging. Neutrons interact not only with the nuclei of the materials but also with the magnetic moments of the atoms. In ferromagnetic materials, this magnetic interaction is constructive. The separation between magnetic and nuclear scattering was performed by using the different dependence on the azimuthal angle $\alpha$ between the scattering vector $\boldsymbol{Q}$ and the vector of the sample magnetization $M$ of the two intensity components [4] by application of the program ancos2 developed by Gosh from the ILL Grenoble.

$$\left(\frac{\mathrm{d}\Sigma(\boldsymbol{Q})}{\mathrm{d}\Omega}\right) = \left(\frac{\mathrm{d}\Sigma(\boldsymbol{Q})_{\mathrm{nuc}}}{\mathrm{d}\Omega}\right) + \left(\frac{\mathrm{d}\Sigma(\boldsymbol{Q})_{\mathrm{mag}}}{\mathrm{d}\Omega}\right) \tag{1}$$

$$\left(\frac{\mathrm{d}\Sigma(\boldsymbol{Q})_{\mathrm{nuc}}}{\mathrm{d}\Omega}\right) \sim \Delta\eta^2_{\mathrm{nuc}} \tag{2}$$

$$\left(\frac{\mathrm{d}\Sigma(\boldsymbol{Q},\alpha)_{\mathrm{mag}}}{\mathrm{d}\Omega}\right) \sim \Delta\eta^2_{\mathrm{mag}} \sin^2(\alpha). \tag{3}$$

$(\mathrm{d}\Sigma(\boldsymbol{Q})/\mathrm{d}\Omega)$ is the macroscopic differential nuclear and magnetic scattering cross-section, respectively, and $\Delta\eta$ the difference between the mean scattering densities of inhomogeneities and of the matrix which is given by

$$\Delta\eta = n_{\mathrm{I}} b_{\mathrm{I}} - n_{\mathrm{M}} b_{\mathrm{M},} \tag{4}$$

$n_{\mathrm{I,M}}$ are the mean number densities of atoms and $b_{\mathrm{I,M}}$ their mean scattering lengths of in the inhomogeneity or matrix, respectively. In dia- or paramagnetic phases the magnetic moments are disordered. $b_{\mathrm{I,mag}}$ is in this case zero. It means that the scattering density of non-ferromagnetic phases in a ferromagnetic matrix is zero and the magnetic scattering does not depend on the structure and composition of this phase, only on the known structure of the matrix. The radial averaging of the magnetic scattering was performed as a projection of the scattering to $\alpha = \pi/2$:

$$\frac{\mathrm{d}\Sigma(\boldsymbol{Q})_{\mathrm{mag}}}{\mathrm{d}\Omega} = \int_{\alpha=0}^{2\pi} \frac{\mathrm{d}\Sigma(\boldsymbol{Q},\alpha)_{\mathrm{mag}}}{\mathrm{d}\Omega} / \sin^2(\alpha)\mathrm{d}\alpha \sim \Delta\eta^2_{\mathrm{mag}}. \tag{5}$$

From these data sets the size distribution function as the volume distribution $D_{\mathrm{V}}(R)$ was calculated using the indirect transformation method developed by Glatter [5]:

$$\left(\frac{\mathrm{d}\Sigma(\boldsymbol{Q})_{\mathrm{mag,nuc}}}{\mathrm{d}\Omega}\right) = k\int_0^\infty D_{\mathrm{V}}(R) R^3 \ \ \Delta\eta^2(R)_{\mathrm{mag,nuc}} \Phi(\boldsymbol{Q},R)\mathrm{d}R. \tag{6}$$

$k$ is a constant depending on the shape of the inhomogeneities, $R$ the characteristic dimension of them, The so-called shape factor $\Phi(\boldsymbol{Q},R)$ is the Fourier transform of the shape of the inhomogeneities. If there are more than one type of inhomogeneities with different size and structure then $\Delta\eta$ depends on $R$. Eq. (5) is only properly valid if inhomogeneities seen by the nuclear scattering are identical in shape and size with the inhomogeneities seen by the magnetic scattering. Otherwise different functions for $D_{\mathrm{V}}(R)$ and $\Phi(\boldsymbol{Q},R)$ have to be taken into account.

The indirect transformation method estimates $D_{\mathrm{V}}$ under the boundary condition that $D_{\mathrm{V}}(R)$ is unequal to zero only in the range $0 \le R \le \pi/Q_{\min}$ and for a supposed shape of the inhomogeneities. For this analysis Glatter's ITP92 software was used. $D_{\mathrm{V}}$ was calculated by the presumption of globular inhomogeneities.

## 3. Results

Figs. 1 and 2 show the magnetic and nuclear scattering of three states of the material ESW-A. The small angle

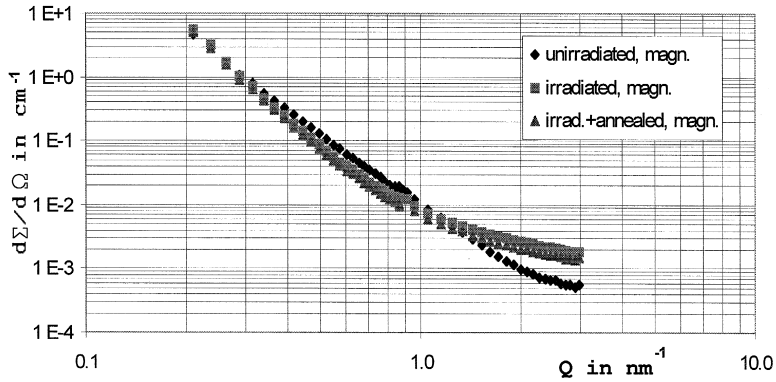


Fig. 1. Magnetic small angle neutron scattering of the unirradiated, the irradiated and the irradiated + annealed (270°C) states of material ESW-A.

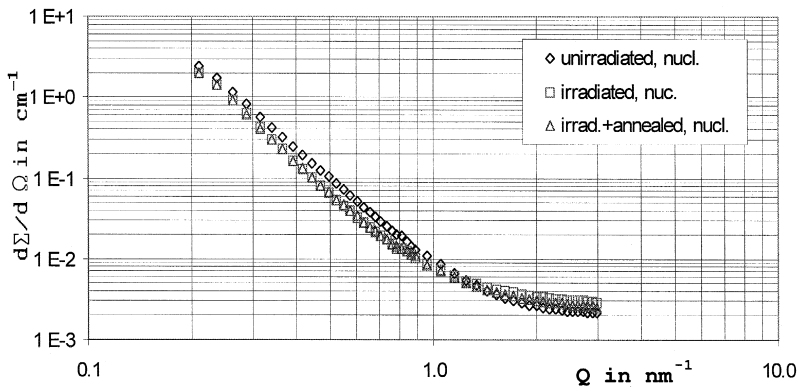


Fig. 2. Nuclear small angle neutron scattering of the unirradiated, the irradiated and the irradiated + annealed (270°C) states of material ESW-A.

scattering pattern of this material is also typical for ESW-C. Large differences in the magnetic scattering were found preferentially at higher values of $\boldsymbol{Q}$.

The measured differential scattering cross-section $(\mathrm{d}\Sigma(\boldsymbol{Q})/\mathrm{d}\Omega)_{\mathrm{mes}}$ does not only contain the $\boldsymbol{Q}$-dependent small angle neutron scattering $(\mathrm{d}\Sigma(\boldsymbol{Q})/\mathrm{d}\Omega)_{\mathrm{SAS}}$, but also

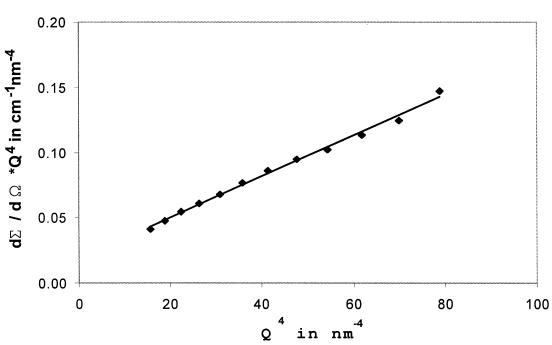


Fig. 3. $(\mathrm{d}\Sigma(\boldsymbol{Q})/\mathrm{d}\Omega)_{\mathrm{mes}}\boldsymbol{Q}^4$ vs. $\boldsymbol{Q}^4$ plot for the estimation of the constant scattering contribution (magnetic scattering of the irradiated state of ESW-A).

a constant contribution $(\mathrm{d}\Sigma/\mathrm{d}\Omega)_{\mathrm{c}}$. This constant contribution is caused by the incoherent scattering, mainly of the different iron isotopes, and by the monotonic Laue scattering of point defects in the matrix. The constant scattering contribution $(\mathrm{d}\Sigma/\mathrm{d}\Omega)_{\mathrm{c}}$ increases after the irradiation and decreases slightly through the following post-irradiation annealing. The changes due to irradiation and annealing are stronger in the constant magnetic scattering than in the nuclear scattering. In order to seperate $(\mathrm{d}\Sigma/\mathrm{d}\Omega)_{\mathrm{c}}$ from $(\mathrm{d}\Sigma(\boldsymbol{Q})/\mathrm{d}\Omega)_{\mathrm{SAS}}$ the asymptotic behaviour of $(\mathrm{d}\Sigma(\boldsymbol{Q})/\mathrm{d}\Omega)_{\mathrm{SAS}}$ can be utilized. At $\boldsymbol{Q}$-values of $\boldsymbol{Q} \geq 4/R$ the differential scattering cross-section for inhomogeneities with a well-defined interface to the matrix (no fractal structures or dislocations) and without preferred orientation decreases with increasing $\boldsymbol{Q}$ according to the power law:

$$\left(\frac{\mathrm{d}\Sigma}{\mathrm{d}\Omega}\right)_{\mathrm{SAS}} = \frac{2\pi c \ \ \Delta\eta^2 S}{Q^4} = PQ^{-4}, \tag{7}$$

where $c$ is the concentration of the inhomogeneities, $S$ is the surface of the inhomogeneity and $P$ is the well known

Table 3
Constant scattering contribution for the investigated materials

| $(d\Sigma/d\Omega)_c$ ($cm^{-1}$) | ESW-A | | | ESW-C | | |
|---|---|---|---|---|---|---|
| | unirradiated | irradiated | irradiated + annealed | unirradiated | irradiated | irradiated + annealed |
| nuclear | 0.0020056 | 0.002728 | 0.002440 | 0.002184 | 0.002530 | 0.002328 |
| magnetic | 0.000430 | 0.001588 | 0.001245 | 0.000499 | 0.001518 | 0.001414 |

Porod constant. The measured differential scattering cross-section $(d\Sigma(\boldsymbol{Q})/d\Omega)_{mes} = (d\Sigma(\boldsymbol{Q})/d\Omega)_{SAS} + (d\Sigma/d\Omega)_c$ can be multiplied by $\boldsymbol{Q}^4$:

$$\left(\frac{d\Sigma(\boldsymbol{Q})}{d\Omega}\right)_{mes}\boldsymbol{Q}^4 = \left(\frac{d\Sigma(\boldsymbol{Q})}{d\Omega}\right)_{SAS}\boldsymbol{Q}^4 + \left(\frac{d\Sigma}{d\Omega}\right)_c\boldsymbol{Q}^4 = P + \left(\frac{d\Sigma}{d\Omega}\right)_c\boldsymbol{Q}^4. \quad (8)$$

Fig. 3 shows the $(d\Sigma(\boldsymbol{Q})/d\Omega)_m\boldsymbol{Q}^4$ vs. $\boldsymbol{Q}^4$ plot of the measured magnetic scattering of the ir-radiated state of material ESW-A. The good agreement between the measured data and the linear dependence predicted by the theory shows that the made assumptions are fulfilled. The slope of the curve is $(d\Sigma/d\Omega)_c$. Table 3 gives the values of the constant scattering contribution for both materials.

The subtraction of the constant scattering contribution from the measured differential scattering cross-section yields the actual small angle scattering cross-section. Fig. 4 compares the nuclear and the magnetic small angle

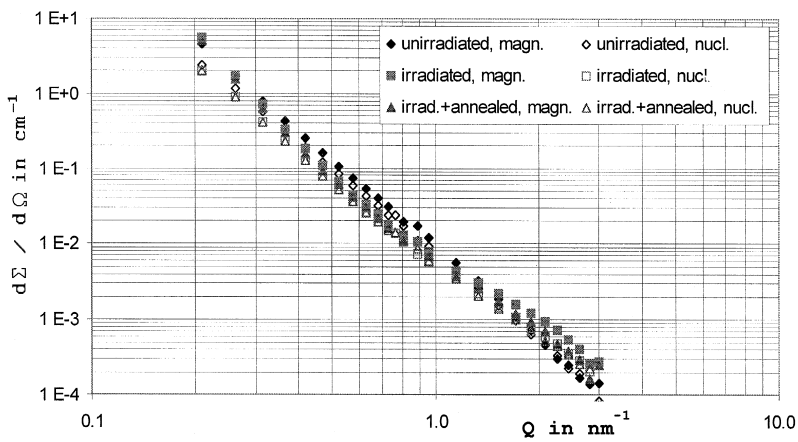


Fig. 4. Corrected magnetic and nuclear small angle neutron scattering of the different states of material ESW-A.

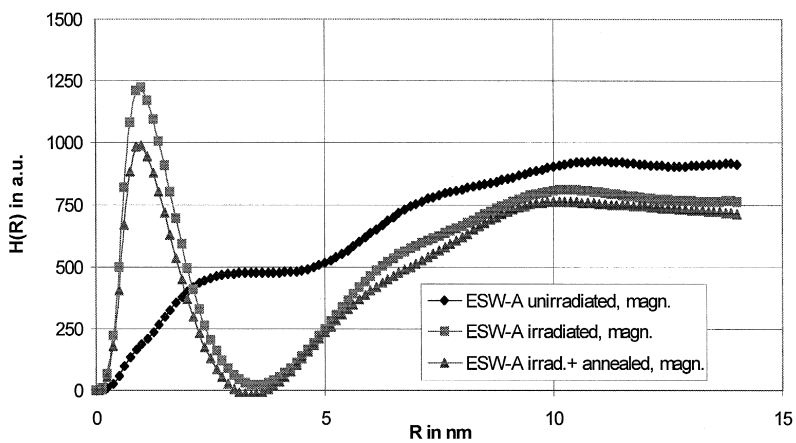


Fig. 5. Volume distribution function of the unirradiated, irradiated and irradiated + annealed (270°C) state of the material ESW-A, calculated from the magnetic SANS.

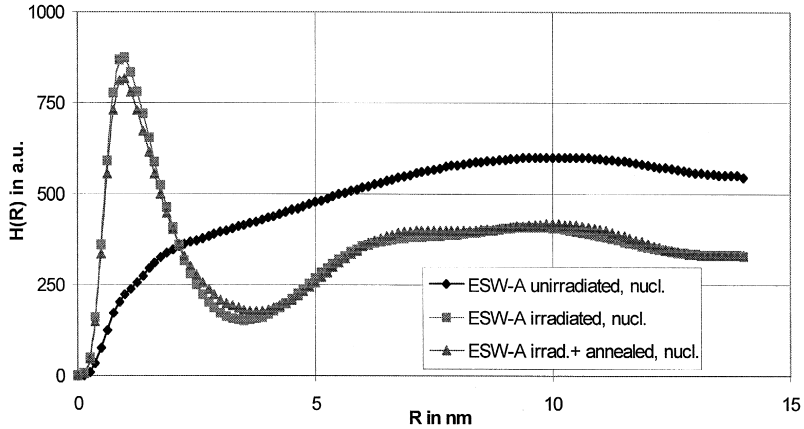


Fig. 6. Volume distribution function of the unirradiated, irradiated and irradiated + annealed (270°C) state of the material ESW-A, calculated from the nuclear SANS.

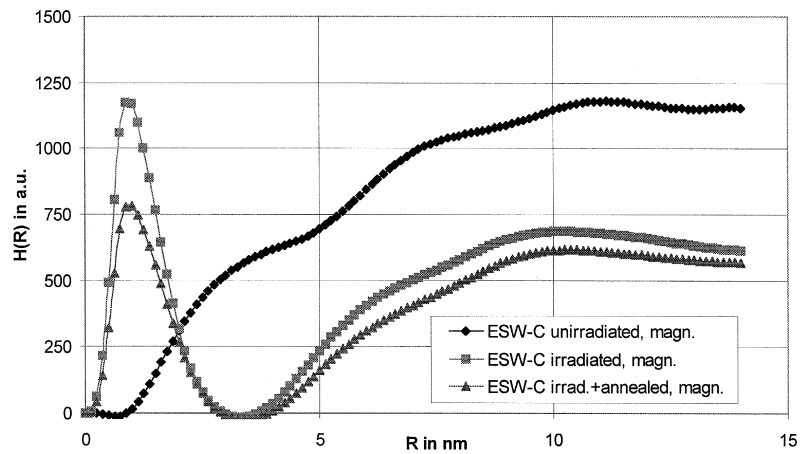


Fig. 7. Volume distribution function of the unirradiated, irradiated and irradiated + annealed (270°C) state of the material ESW-C, calculated from the magnetic SANS.

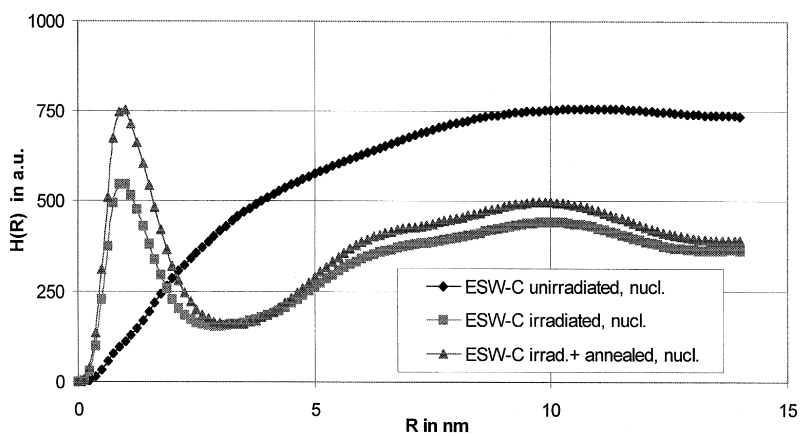


Fig. 8. Volume distribution function of the unirradiated, irradiated and irradiated + annealed (270°C) state of the material ESW-C, calculated from the nuclear SANS.

neutron scattering cross-section of the different states of the material ESW-A after this correction. From these SANS data the volume distribution functions for the several material states are calculated using the indirect transformation method. As the program ITP92 does not allowed an absolute calibration, the results are given as the function $H(R)$, which is connected by an unknown calibration factor f with the product of difference in the scattering density $\Delta\eta(R)$ and volume distribution function $D_V(R)$:

$$H(R) = f \quad \Delta\eta D_V(R) \tag{9}$$

The results for the nuclear and the magnetic inhomogeneities in the different states of the materials ESW-A and ESW-C are given in Figs. 5–8. The upper limits of the size distribution functions at 14 nm are set by the boundary condition of the indirect transformation method.

## 4. Discussion

### 4.1. Constant scattering contribution

The constant scattering contribution can be estimated by

$$\left(\frac{\mathrm{d}\sigma}{\mathrm{d}\Omega}\right)_c = \frac{\rho}{2}\sum_{\mu,\nu}\left(b_\mu - b_\nu\right)^2 c_\mu c_\nu = \rho\left(\overline{b^2} - \overline{b^2}\right) \tag{10}$$

with $\rho$ being the number density of the atoms in the lattice. $\mu$ and $\nu$ are the indices of the different isotopes, $b$ is the scattering length of the isotopes and $c$ their concentration. The symbol—indicates the mean value over all kinds of isotopes.

In the unirradiated state, the constant scattering is mainly caused by the incoherent scattering of the different iron isotopes. The different iron isotopes only cause nuclear scattering as they have the same magnetic behaviour. The theoretical value of this nuclear scattering should be $(\mathrm{d}\Sigma/\mathrm{d}\Omega)_{\text{c-Fe}} = 0.0027\ \mathrm{cm}^{-1}$. The upper limit is 0.0037 $\mathrm{cm}^{-1}$ for the case that each foreign atom is solved in the iron lattice. The measured values for the unirradiated state are sligthly smaller than the expected value. Small uncertainties in the calibration and in the background correction could be the reason for this difference. The magnitude of the constant scattering contribution is small, thus the relative error is high. These uncertainties are systematical and should be the same for all materials. Therefore, only the changes in the constant scattering contribution, not the absolute values are discussed. The very small value for magnetic constant scattering contribution confirms that the constant scattering in the unirradiated state is mainly caused by the iron isotopes.

The isotope composition is not significantly changed by the irradiation. Consequently, the increase of the constant scattering contributions after the irradiation at low temperature is due to the increase of the number of point defects. The differences between the increase in the magnetic and the nuclear scattering can provide clues about the kind of point defects. The stronger increase of the constant magnetic scattering compared to constant nuclear scattering can be caused by the following.

(1) change in the oxidation state of iron, copper or nickel that transforms the ferromagnetic or diamagnetic behaviour into a paramagnetic behaviour. Paramagnetism results in a completely incoherent magnetic scattering behaviour. Nuclear scattering is not affected by this chemical change. An irradiation-induced change in the oxidation state in the bulk of the material is not probable. However, surface effects cannot be absolutely excluded. These effects should be more or less random and cannot explain the similar behaviour of both materials.

(2) formation of new point defects which stronger differ to the iron matrix in the magnetic scattering length $b_m$ than in the nuclear scattering length $b_n$. Such point defects can be, for instance, copper ($\Delta b_n = 0.173 \times 10^{-12}$ cm, $\Delta b_m = 0.585 \times 10^{-12}$ cm) or nickel ($\Delta b_n = 0.085 \times 10^{-12}$ cm, $\Delta b_m = 0.34 \times 10^{-12}$ cm). This explanation seem to be more probable.Nevertheless, the formation of voids would cause a stronger increase of the nuclear scattering ($\Delta b_n = 0.945 \times 10^{-12}$ cm, $\Delta b_m = 0.585 \times 10^{-12}$ cm). However, the formation of vacancies cannot be excluded.

### 4.2. Size distribution of precipitates

The shape of the size distribution functions calculated from the magnetic and from the nuclear scattering as well as the position of their peaks are very similar for the several material states. Only the height of the peaks differ. This is caused by the differences between the nuclear and magnetic scattering densities. It shows that Eq. (5) is properly fulfilled. No differences in the principle shape of the size distribution functions are found for the two materials.

In the unirradiated state, the distribution is smooth without a sharp peak. At high $R$-values the detection limit caused by the used $\boldsymbol{Q}$-range limits the curves. It means that larger inhomogeneities are also be present in the materials. This distribution corresponds to vanadium rich MC or $M_4C_3$ precipitates which can be found by transmission electron microscopy (TEM) [6]. In Ref. [6], the maximum of the size distribution of these carbides was estimated with $D = 2R = 17$ nm for a 15 Kh2MFA steel. Due to the higher content of vanadium the number of these precipitates is higher in ESW-C than in ESW-A.

The ratio between nuclear + magnetic and nuclear scat-

tering, the so-called $A$-ratio [7], can provide information about the type of inhomogeneities. It is defined as follows:

$$A = \frac{\left(\frac{d\sigma(\boldsymbol{Q})_{nuc}}{d\Omega}\right)_{SAS} + \left(\frac{d\sigma(\boldsymbol{Q})_{mag}}{d\Omega}\right)_{SAS}}{\left(\frac{d\sigma(\boldsymbol{Q})_{nuc}}{d\Omega}\right)_{SAS}}$$

a system with only one type of inhomogeneities follows from Eqs. (2) and (3):

$$A = \frac{\Delta\eta_{nuc}^2 + \Delta\eta_{mag}^2}{\Delta\eta_{nuc}^2}. \quad (11)$$

For systems with different types of inhomogeneities $\Delta\eta$ depends on $R$. Then $A$ also depends on $R$ and, thus, also on $\boldsymbol{Q}$. The $A$-ratio for the different types of inhomogeneities can be estimated from the ratio of the size distribution functions $H$ calculated from the nuclear and the magnetic scattering. For the wide distribution found in the unirradiated state an $A$-ratio of 2.5 was calculated for both materials. This is near to the theoretical value of vanadium carbide VC ( $A = 2.4$).

After irradiation the number of this kind of precipitates decreases. This decrease is stronger for material ESW-C than for ESW-A. Additionally, there is, however, a large number of precipitates with sizes between 0.3 and 3.0 nm and a maximum at about 1.0 nm. This is in agreement with TEM results, where non-resoluble black dots with a size smaller than 8 nm were found [8]. The lower range limit reaches the atomic distance. It means that the new structures formed by the irradiation consist of few to 1000 atoms. Due to the higher fluence, the maximum is slightly higher for ESW-A. For these peaks, $A$-ratios of 3.0 and 3.2 were estimated for material ESW-A and ESW-C, respectively.

Such newly formed defects could be small precipitates or voids with a content of solutes. The process of Cu precipitation could also be of importance. Cu precipitation is impeded in the as-received state due to kinetic reasons. Under irradiation, Cu precipitation can be continued to equilibrium with high speed due to the enhanced diffusion. The comparison of the first peak of the size distribution shows that such an effect must be considered. Although the fluence for ESW-A is higher than twice the fluence for ESW-C, the height of the peaks is comparable. This fact and the higher $A$-ratio estimated for this peak could be caused by a higher portion of Cu precipitation in the Cu rich material ESW-C. Additionally a refinement of MC precipitates compared with a changing of their chemical composition (increase of the iron content effects an increasing of the $A$-value) could be a possible reason of this effect.

The magnetic scattering data show that after post-irradiation annealing the number of precipitates with a size smaller than 3.0 nm decreases, particularly in material ESW-C, whereas the shape of the size distribution function keeps unchanged. On the other hand the peak in the size distribution function calculated from the nuclear scattering is not changed significantly for material ESW-A and increase for material ESW-C after the annealing. The $A$-ratios of these peaks decrease down to 2.2 and 2.0 for ESW-A and ESW-C, respectively. This shows that in addition to the decreasing number of inhomogeneities an increase of $\Delta\eta$ occurs. This effect can be caused by an improvement of the structure of the irradiation-induced precipitates for instance by decreasing the iron content of small carbides. The increase in $\Delta\eta$ is stronger for ESW-C than for ESW-A.

The results can be explained by a partial dissolution of precipitates formed by the metallurgical process in the collision cascade. Vacancies are also formed in the iron lattice. Some of the atoms, which are knocked out from the precipitates by the collision process remain in the iron lattice as point defects. The others with a higher mobility can rearrange to new small precipitates or voids. After the annealing treatment the vacancies are trapped and some of the newly formed inhomogeneities are dissolved and their structure is changed.

## 5. Conclusions

The effect of low temperature neutron irradiation on the formation of precipitates and point defects was studied by small angle neutron scattering for two laboratory heats of the VVER-440-type RPV steel 15 Kh2MFA. The results are as follows.

(1) Differences in the content of silicon, vanadium and copper do not influence the principal mechanisms but the intensity of the process which forms the irradiation-induced precipitates.

(2) The number of point defects is increased by the irradiation at low temperature. The point defects are not only vacancies but also resolved atoms from precipitates formed in the metallurgical process.

(3) The number of the precipitates, which exist in the unirradiated state, decreases by irradiation. A partial dissolution of these precipitates occurs. Smaller inhomogeneities with sizes between 0.3 and 3.0 nm are formed.

(4) After annealing near to the service temperature of a nuclear reactor the number of point defects slightly decreases but is always higher than in the unirradiated state. The assumption, that vacancies are trapped at this temperature but resolved atoms stay in the iron lattice, can explain the effect.

(5) Annealing decreases the number and changes the structure of the irradiation-induced inhomogeneities. The precipitates, which exist in the unirradiated state, are hardly affected by this thermal treatment.

## Acknowledgements

The authors thank Mrs M.-H. Mathon from LLB Saclay and Mr F. Eichhorn from FZ Rossendorf for their helpful discussion of the results.

## References

[1] T. Diaz dela Rubia, M.W. Guinan, Mater. Res. Forum 97–99 (1992) 23.
[2] K.C. Russell, J. Nucl. Mater. 206 (1993) 129.
[3] Neutron-Scattering Instrumentation at the Research Reactor BER II, Berlin Neutron Scattering Center—BENSC, May 1996.
[4] G. Brauer, F. Eichhorn, F. Frisius, R. Kampmann, ASTM-STP 1175 (1993) 503.
[5] O. Glatter, J. Appl. Crystallogr. 13 (1980) 7.
[6] K. Törrönen, Microstructural Parameters and Yielding in a Quenched and Tempered Cr–Mo–V Pressure Vessel Steel, Materials and Processing Technology Publication 22, Technical Research Centre of Finland, Espoo 1979.
[7] M. Grosse, F. Eichhorn, J. Boehmert, G. Brauer, ASTM-STP 1270 (1996) 1123.
[8] J. Kocik, E. Keilova, J. Nucl. Mater. 172 (1990) 126.